Int. J. Electron. Commun. (AEÜ) 156 (2022) 154406

Contents lists available at ScienceDirect

International Journal of Electronics and Communications

journal homepage: www.elsevier.com/locate/aeue

Regular paper

An improved cascode common-source LNA with inductive source degeneration for RF applications

Farshad Gozalpour [a], Maryam Dodangeh [a], Mohammad Yavari [a,*], Ali Mirvakili [b]

[a] Integrated Circuits Design Laboratory, Department of Electrical Engineering, Amirkabir University of Technology (Tehran Polytechnic), P.O. 15875-4413, Tehran, Iran
[b] Department of Electrical Engineering, Yazd University, Yazd, Iran

ARTICLE INFO

Keywords:
CMOS low-noise amplifiers (LNAs)
Cascode common-source LNA
Inductive source degeneration
Volterra series linearity analysis
Power gain

ABSTRACT

This paper presents a novel structure to enhance the power gain (S_{21}) of the conventional cascode common-source (CS) low-noise amplifier (LNA) with inductive source degeneration. The proposed LNA has an extra transistor and a capacitor in comparison with the conventional structure. The additive transistor significantly increases the S_{21} of the conventional cascode CS LNA with inductive source degeneration with the same DC power consumption (P_{DC}), third-order input intercept point (IIP3), area, and slightly lower noise figure (NF). The utilized capacitor is used to improve the IIP3 of the proposed LNA. The power gain improvement of the proposed LNA has been validated by both theoretical analysis and extensive post-layout simulation results. The proposed and conventional LNAs have been designed in TSMC 180 nm CMOS technology. The post-layout simulation results of the proposed LNA are 2.42 dB NF, S_{21} of 15.55 dB, and 0.84 dBm IIP3 while consuming 3.2 mW from 1.2 V power supply. The simulated S_{21} of the proposed LNA is about 2.55 dB (34.2 %) larger than the conventional cascode LNA with the same other performance parameters. Also, the achieved figure-of-merit (FoM) of the proposed LNA is substantially larger than the conventional cascode CS LNA with inductive source degeneration.

1. Introduction

Low-noise amplifiers (LNAs) play a dominant role as the first stage in radio frequency (RF) receivers [1,2]. They must have sufficient voltage gain in order to reduce the input-referred noise of the following stages, and they also must have a low noise figure (NF) [3–12]. Moreover, they need to have low DC power consumption (P_{DC}). The cascode common-source (CS) topology with inductive source degeneration has been widely used in LNA implementations in previous works due to its suitable features [13–21]. It can provide input impedance matching with low NF. Its power consumption is also acceptable, and it is almost stable [22].

State-of-the-art papers in literature demonstrate a variety of techniques to enhance the performance of cascode CS LNA in different terms, such as DC power consumption, gain, linearity, and noise. In [14], the third-order input intercept point (IIP3) of a sub-threshold biased cascode CS LNA is improved by using an inductor between the power supply and the gate of the cascode transistor. Also, a digitally controlled capacitor is utilized between the drain and gate terminals of the cascode transistor. Several techniques including the forward body biasing, current reuse, and input feedback capacitor have been utilized in [15] to improve the performance of the cascode CS LNA with inductive degeneration. In [16,17], the simultaneous and balanced optimization of input matching and NF is investigated in cascode CS LNA with consideration for substrate and metal loss effects of inductors.

In [23], a balun has been combined with dual-path noise and nonlinearity cancellation techniques to reduce the NF and improve the gain with low power consumption. However, compared to the conventional CS inductively degenerated LNA, the achieved IIP3 is deteriorated by 2.7 dB mainly due to the passive voltage gain of the balun. In [24], the dual feedback, current-reuse, and forward body biasing schemes are utilized in the cascode CS LNA to realize a reconfigurable multi-band LNA with low power dissipation. The body self-biasing scheme is also employed in [19] in a differential multi-band cascode CS structure to reduce the noise contribution caused by the body effect of MOS transistors. A low-power variable-gain cascode LNA has been proposed in [25] using several design optimization techniques. In [26], the impact of source-bulk and drain-bulk capacitors is neutralized by using the bulk isolation technique. To do so, a large resistor is added between the bulk and ground nodes of each transistor. By this way, the power gain of each

* Corresponding author.
E-mail address: myavari@aut.ac.ir (M. Yavari).

https://doi.org/10.1016/j.aeue.2022.154406
Received 15 April 2022; Accepted 30 August 2022
Available online 5 September 2022

transistor is enhanced. Using the bulk isolation technique, a two-stage cascode LNA has been realized in 65 nm CMOS for mm-wave frequencies in [26].

In this paper, the main focus is to enhance the power gain (S_{21}) of the conventional cascode CS LNA with inductive source degeneration without any deterioration in other parameters. By adding a transistor and using an extra capacitor in the conventional structure, a significant improvement in the power gain is obtained in comparison with the conventional cascode CS LNA with almost the same other performance metrics, power consumption, and area. The proposed technique can be also utilized in all inductively source degenerated CS LNAs as well to further enhance the power gain, and hence, the overall performance.

The rest of the paper is organized as follows. Section 2 describes the structure of the proposed LNA and provides an extensive gain, noise, and linearity analysis. Section 3 provides the post-layout simulation results and also a comprehensive comparison with several state-of-the-art LNAs. Finally, conclusions are given in Section 4.

2. Structure of the proposed LNA

The schematic of the proposed LNA is depicted in Fig. 1, where the M_3 transistor is added to the conventional cascode CS LNA with inductive source degeneration. Transistor M_b and resistors R_{b1} and R_{b2} are used to define the bias current of the main M_1, M_2, and M_3 transistors. C_n is a bypass capacitor which is used to cancel the thermal noise effect of the biasing circuit. L_P is the bondwire inductor, and C_P is used to model the capacitance of the input pad and input pin to the ground. C_a is an added parallel capacitor to C_{gs} of the M_1 transistor in order to achieve a realizable value for the on-chip L_S inductor. Also, C_b is an added parallel capacitor to C_{gs} of the M_3 transistor in order to improve the value of IIP3 in the proposed LNA. Indeed, using C_b adds one degree of freedom to increase the value of IIP3 as will be discussed more in Section 3. In addition to C_b, the difference between the structure of the proposed LNA and the conventional cascode LNA is in using the M_3 transistor, which is highlighted with blue color in Fig. 1. To be more specific, the suggested circuit has two M_1 and M_3 transistors, which play the role of M_1 transistor in the conventional circuit. In the proposed LNA, the size of M_1 and M_3 transistors is the same and it is half the size of M_1 transistor in the conventional cascode CS LNA. This is needed to have the same current density in all transistors at both structures, and hence, to provide a fair comparison between them.

2.1. Gain analysis

In order to separate the parameters in the following analysis, subscripts p and c are used for the proposed and conventional LNAs, respectively. In the proposed LNA, the small-signal gate-source voltage of M_3 transistor is more than that of M_1 transistor since it is equal to the summation of the gate-source voltage of M_1 transistor and the voltage across the L_S inductor. Therefore, in the proposed LNA, the ac voltage drop across L_S is used to increase the small-signal current of M_3. On the other hand, the DC overdrive voltage of M_1 and M_3 transistors is almost the same since the DC voltage drop across the inductor L_S is negligible and the transistors M_1 and M_3 have the same aspect ratio. Therefore, $g_{m3,p}$ is very close to $g_{m1,p}$. So, based on this technique, although the size of M_1 and M_3 transistors is the same and it is half of the M_1 transistor in the conventional LNA, the overall small-signal current is larger than the conventional LNA which results in higher power gain.

As illustrated in Fig. 2(a), by denoting the transconductance of M_1 transistor in the conventional cascode CS LNA by $g_{m1,c}$, its voltage gain at the same resonance frequency of the input matching and output load networks is given by [22]:

$$A_{v,conv.} = Q_c\, g_{m1,c} R_L \tag{1}$$

where

$$Q_c = \frac{1}{2R_S C_{gs1,c}\omega_{0,c}}, \quad \omega_{0,c} = \frac{1}{\sqrt{(L_S + L_G + L_P)C_{gs1,c}}} \tag{2}$$

In relation (1), R_L is the resistance of L_D due to its finite quality factor and $C_{gs1,c} = C_{gs,M1} + C_a$, where $C_{gs,M1}$ is the gate-source capacitance of M_1 transistor.

It is worth mentioning that C_b is small (45 fF in the designed LNA). So, to find the gain of the proposed LNA, the $C_{gs3,p} = C_{gs,M3} + C_b$ is neglected for simplicity. By writing KCL at the gate of M_1 transistor in Fig. 2(b), we have:

$$V_{gs1} = Q_p V_{in} \quad => \quad \frac{V_{in} - (V_1 + Q_p V_{in})}{R_S + s\ L_{GT}} = sC_{gs1,p}\, Q_p\, V_{in} \tag{3}$$

where

$$Q_p = \frac{1}{2R_S C_{gs1,p}\omega_{0,p}}, \quad \omega_{0,p} = \frac{1}{\sqrt{(L_S + L_G + L_P)C_{gs1,p}}} \tag{4}$$

In relation (4), $C_{gs1,p} = C_{gs,M1} + C_a$. At the resonance frequency of the input matching network of the LNA, $C_{gs1,p}\,(L_{GT} + L_S)s^2 + 1 = 0$ and since $L_{GT} = L_P + L_G$ is normally much larger than L_S to reduce the NF [22], as it is also used in the designed LNA, the approximation of $C_{gs1,p}\,(L_{GT} + L_S) \approx C_{gs1,p}\ L_{GT} \approx \omega_{0,p}^{-2}$ is considered. Based on this approximation, V_1 is simplified as:

$$V_1 \approx V_{in}\left(1 - sC_{gs1,p} Q_p\, R_S\right) \tag{5}$$

By writing KCL at the drain of M_1 transistor in Fig. 2(b), we have:

$$I_{out} = g_{m1,p} Q_p V_{in} + g_{m3,p}\left(V_1 + Q_p\ V_{in}\right) \tag{6}$$

So, by substituting the relation (5) into the relation (6), I_{out} is obtained as:

$$I_{out} = V_{in}\left[Q_p\left(g_{m1,p} + g_{m3,p}\right) + g_{m3,p} - jQ_p g_{m3,p} C_{gs1,p} R_S \omega_{0,p}\right] \tag{7}$$

As it was mentioned before, since the size and drain current of M_1

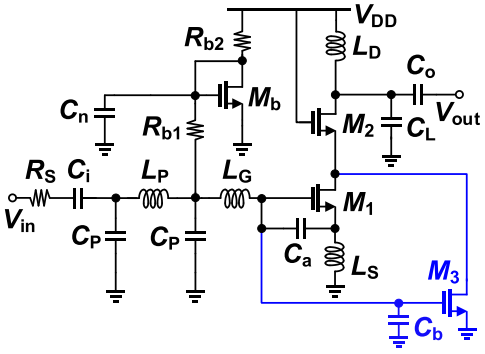

Parameter	Value	Parameter	Value
$(W/L)_{1,3}$	12×7.2 µm / 0.18 µm	C_o	0.5 pF
$(W/L)_2$	24×7.2 µm / 0.18 µm	C_a	220 fF
$(W/L)_b$	4.44 µm / 0.18 µm	C_n	1 pF
R_{b1}	33 kΩ	C_b	45 fF
R_{b2}	11 kΩ	L_S	1 nH
C_i	2 pF	L_P	1 nH
C_P	50 fF	L_G	8.16 nH
C_L	235 fF	L_D	4.07 nH

Fig. 1. Schematic of the proposed LNA with simulated device parameters.

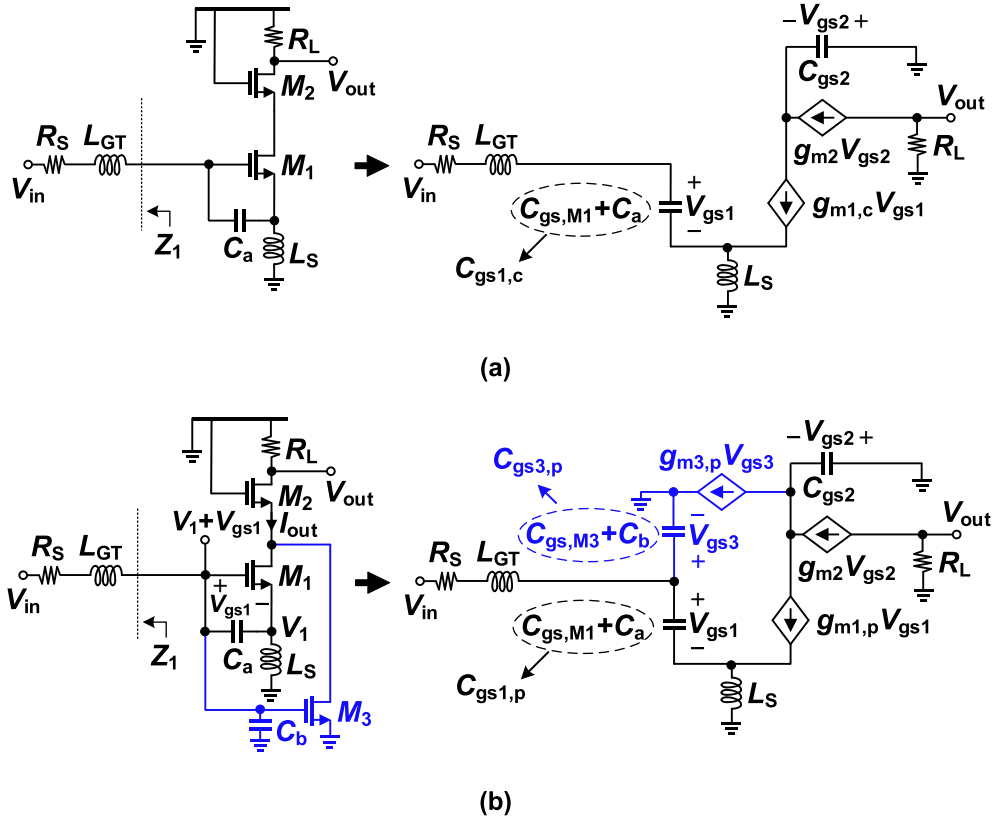

Fig. 2. Equivalent circuit and small-signal model for gain and linearity analysis. (a) conventional LNA, and (b) proposed LNA.

and M_3 transistors is half that of the transistor M_1 in the conventional cascode LNA (i.e., $g_{m1,p} = g_{m1,c}/2$) and assuming that $g_{m1,p}$ is almost equal to $g_{m3,p}$, the relation (7) is simplified as below:

$$I_{out} = V_{in}\left[Q_p g_{m1,c} + \frac{1}{2}g_{m1,c} - \frac{1}{2}jQ_p g_{m1,c} C_{gs1,p} R_S \omega_{0,p}\right] \tag{8}$$

By inserting the amount of Q_p in the imaginary part in relation (8), it becomes equal to $g_{m1,c}/4$ that is smaller than the real part in (8). So, to reveal a simpler equation, the imaginary part can be neglected in comparison to the real part, and the gain of the proposed LNA is almost given by:

$$\begin{aligned} A_{v,prop.} &= \sqrt{\left(Q_p g_{m1,c} R_L + \frac{1}{2}g_{m1,c}R_L\right)^2 + \left(\frac{1}{4}g_{m1,c}R_L\right)^2} \\ &\approx Q_p g_{m1,c} R_L + \frac{1}{2}g_{m1,c}R_L \end{aligned} \tag{9}$$

It is worth mentioning that since the size of M_1 transistor in the proposed LNA is half that of M_1 transistor in the conventional LNA, $C_{gs,M1}$ in the proposed LNA is half that of $C_{gs,M1}$ in the conventional LNA. However, since C_a is larger than $C_{gs,M1}$, $C_{gs1,c}$ and $C_{gs1,p}$ are mostly determined by C_a ($C_{gs1,p}$ is a little smaller than $C_{gs1,c}$). So, as long as the conventional circuit and the suggested LNA have similar C_a, Q_p is almost equal to Q_c, that results in:

$$A_{v,prop.} \approx Q_c g_{m1,c} R_L + \frac{1}{2}g_{m1,c}R_L \tag{10}$$

According to the relations (1) and (10), the gain of the proposed LNA is greater than the conventional cascode CS LNA since it has an additional term which is equal to (1/2) $g_{m1,c}$ R_L.

The gain of a cascode CS LNA with inductive source degeneration is enhanced by reducing the value of source degeneration inductor [22]. This is because, by reducing the value of L_S, the value of $C_{gs1,c}$ should be similarly reduced to maintain the input impedance matching condition. So, according to the relation (2), the value of Q_c is increased resulting in enhanced gain which is given by (1). However, the value of source degeneration inductor cannot be selected very small due to several limitations. Firstly, the degeneration inductor is often realized as a bond wire since it cannot be avoided in a packaged LNA. Therefore, even with a down-bond, the value of degeneration inductor is in the range of 0.5 to 1 nH [22]. Due to this reason, the value of ω_t ($\omega_t \approx g_m/C_{gs}$) of advanced CMOS technologies is artificially reduced by adding an explicit capacitor between the gate and source terminals of a transistor in order to have a reasonable value for degeneration inductor [22]. Secondly, the value of on-chip spiral inductors is usually in the range of 1 to 10 nH and the value control of the small on-chip spiral inductors is difficult due to the parasitic elements.

In the proposed LNA, according to the relation (5), the ac voltage drop across L_S (V_1) is almost independent of the value of L_S when $L_S \ll L_{GT}$ since $C_{gs1,p}Q_p$ is constant for a given value of L_S owing to the input impedance matching condition similar to the conventional LNA. Therefore, according to the relations (6) and (9), the overall gain of the proposed LNA is also increased by reducing the value of L_S. However, the contribution of the added gain term in the proposed LNA will be less since it is almost constant by reducing the value of L_S. So, the usefulness of the proposed gain enhancement technique will be reduced when the value of L_S is reduced. Nonetheless, the value of L_S is in the range of 1 nH and beyond due to its implementation issues. According to the simulation results, with L_S = 1 nH, the power gain improvement of the proposed LNA is about 2.55 dB in comparison with the conventional LNA which is almost a worst case scenario. In other words, the power gain improvement of the proposed LNA can be also more than the reported value if a larger source inductor has been utilized.

2.2. Noise analysis

In the conventional cascode CS LNA, the thermal noise of M_2

transistor can be neglected as it circulates in itself. As a result, M_1 transistor plays the dominant role at the output noise [22]. The NF of the conventional cascode CS LNA with inductive source degeneration due to M_1 and R_L is given by [22]:

$$NF_{conv.} = 1 + \frac{\gamma R_S C_{gs1,c}}{g_{m1,c} L_{GT}} + \frac{4 R_S C_{gs1,c}}{g_{m1,c}^2 R_L L_{GT}} \tag{11}$$

where γ is the excess noise factor. In the proposed LNA, the thermal noise of both M_1 and M_3 transistors should be considered. The circuit shown in Fig. 3 is considered for calculating the noise effect of M_1 transistor at the output. By writing KVL and KCL equations at the gate, drain, and source terminals of transistor M_1, and assuming $g_m r_{ds} \gg 1$, we have:

$$\begin{aligned} &\frac{V_1 + V_{gs1}}{R_S + sL_{GT}} = -sC_{gs1,p} V_{gs1}, \\ &I_{n,out} = g_{m1,p} V_{gs1} + I_{n1} + g_{m3,p}\left(V_{gs1} + V_1\right), \\ &V_1 = sL_S\left[sC_{gs1,p} V_{gs1} + I_{n,out} - g_{m3,p}\left(V_{gs1} + V_1\right)\right] \end{aligned} \tag{12}$$

Owing to the input impedance matching condition, R_S is equal to $g_{m1,p} L_S / C_{gs1,p}$ [22]. Based on this fact, $I_{n,out}$ is obtained as follows:

$$\begin{aligned} I_{n,out} &\approx I_{n1} \times \frac{1 - C_{gs1,p} L_{GT} \omega_{0,p}^2 + jC_{gs1,p} R_S \omega_{0,p}}{2} \\ &= I_{n1} \times \left(\frac{1 - C_{gs1,p} L_{GT} \omega_{0,p}^2}{2} + \frac{j}{4Q_p}\right) \end{aligned} \tag{13}$$

In relation (13), $C_{gs1,p} L_{GT} \omega_{0,p}^2$ is a little smaller than 1. Also, Q_p is larger than 1. Therefore, both real and imaginary parts of the relation (13) are small and only a fraction of the drain thermal noise of M_1 transistor will appear at the output node and it can be neglected in comparison with the noise contribution of M_3 transistor. Actually, the thermal noise current of M_1 transistor creates a noise voltage at the gate of transistor M_3. Then, this noise voltage is converted to the noise current by M_3 which is in an opposite direction with the noise current of M_1 transistor. Hence, the overall noise current due to the thermal noise of transistor M_1 is reduced at the output node. However, the drain current noise of M_3 transistor directly goes to the output node. So, if the noise effect of M_1 transistor is neglected, the NF of the proposed LNA due to M_3 and R_L is approximately given by:

$$\begin{aligned} NF_{Prop.} &\approx 1 + \frac{4kT\gamma g_{m3,p} R_L^2 + 4kTR_L}{4kTR_S\left(2Q_p + 1\right)^2 g_{m3,p}^2 R_L^2} \\ &= 1 + \left(\frac{\gamma R_S C_{gs1,p}}{g_{m1,c} L_{GT}} \times \beta\right) + \left(\frac{4R_S C_{gs1,p}}{g_{m1,c}^2 R_L L_{GT}} \times \frac{\beta}{2}\right) \end{aligned} \tag{14}$$

where

$$\beta = \frac{2}{\left(1 + R_S\sqrt{C_{gs1,p}/L_{GT}}\right)^2} \tag{15}$$

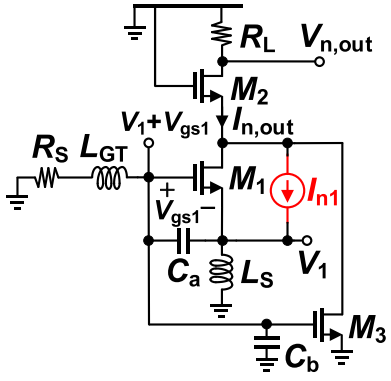

Fig. 3. Equivalent circuit of the proposed LNA used in noise analysis.

As mentioned before, $C_{gs1,p}$ is slightly smaller than $C_{gs1,c}$. Furthermore, β is a little larger than 1. So, the 2nd terms in relations (11) and (14) are almost equal. However, the 3rd term of relation (14) has $\beta/2$ coefficient that is smaller than 1. So, the noise effect of R_L on the NF of the proposed LNA is less than the conventional one, which causes the NF to improve slightly.

2.3. Linearity analysis

The schematic of Fig. 2 has been used for linearity analysis as well. The drain current of M_1 and M_3 transistors, denoted as i_a and i_b, can be modeled by the following equations:

$$\begin{aligned} i_a &= g_{m1,p} v_a + \frac{g_{m1,p}^{'}}{2} v_a^2 + \frac{g_{m1,p}^{''}}{6} v_a^3 \\ i_b &= g_{m3,p} v_b + \frac{g_{m3,p}^{'}}{2} v_b^2 + \frac{g_{m3,p}^{''}}{6} v_b^3 \end{aligned} \tag{16}$$

where g'_m and g''_m are the first- and second-order derivatives of the transistor transconductance (g_m), respectively. The gate-source voltages of M_1 and M_3, i.e. V_a and V_b, and the output current I_{out} can be expressed by the Volterra series in terms of the excitation voltage V_{in} as (17), and (18), respectively [27–32]:

$$\begin{aligned} V_a &= A_1(\omega)^{\circ} V_{in} + A_2(\omega_1, \omega_2)^{\circ} V_{in}^2 + A_3(\omega_1, \omega_2, \omega_3)^{\circ} V_{in}^3 \\ V_b &= B_1(\omega)^{\circ} V_{in} + B_2(\omega_1, \omega_2)^{\circ} V_{in}^2 + B_3(\omega_1, \omega_2, \omega_3)^{\circ} V_{in}^3 \end{aligned} \tag{17}$$

$$I_{out} = E_1(\omega)^{\circ} V_{in} + E_2(\omega_1, \omega_2)^{\circ} V_{in}^2 + E_3(\omega_1, \omega_2, \omega_3)^{\circ} V_{in}^3 \tag{18}$$

Moreover, the IIP3 can be stated as:

$$IIP3(\pm 2\omega_b \mp \omega_a) = \frac{1}{6Re(Z_1(\omega_a))}\left|\frac{E_1(\omega_a)}{E_3(\pm\omega_b, \pm\omega_b, \mp\omega_a)}\right| \tag{19}$$

where $\omega_1 = \omega_2 = \pm\omega_b$, and $\omega_3 = \mp\omega_a$. Assuming that these frequencies are closely spaced, i.e. $\omega_a \approx \omega_b \approx \omega$, the 1st and 3rd order Volterra kernels of the output current, E_1 and E_3, for the proposed and conventional LNAs will be derived by solving the KCL equations at the gate and source nodes of M_1 as (20), and (21), respectively,

$$\begin{aligned} &E_1(\omega_a) = A_1(\omega_a)\left[g_{m1,p} + j\omega_a L_s \gamma(\omega_a) g_{m3,p}\right], \\ &E_3(\pm\omega_b, \pm\omega_b, \mp\omega_a) = \frac{1}{6} A_1(\mp\omega_a) A_1^2(\pm\omega_b) \\ &\times \left\{ \begin{array}{l} \left[g^{''}_{m1,p} - \zeta g^{'2}_{m1,p} \beta(\pm 2\omega_b)\lambda(\pm 2\omega_b)\right]\alpha(\pm\omega) \\ +\left[\omega^2 L_s^2 \gamma(\mp\omega_a)\right]\left[2g^{'}_{m1,3}\lambda(\pm 2\omega_b) + j\omega_b L_s g^{''}_{m3,p}\gamma^2(\pm\omega_b)\right] \end{array} \right\} \end{aligned} \tag{20}$$

$$\begin{aligned} &E_1(\omega_a) = g_{m1,c} A_1(\omega_a), \\ &E_3(\pm\omega_b, \pm\omega_b, \mp\omega_a) = \frac{1}{6} A_1(\mp\omega_a) A_1^2(\pm\omega_b) \\ &\times \left[g^{''}_{m1,c} - \zeta g^{'2}_{m1,c} \beta(\pm 2\omega_b)\lambda(\pm 2\omega_b)\right]\alpha(\pm\omega) \end{aligned} \tag{21}$$

where $g'_{m1,3} = g'_{m1,p} \times g'_{m3,p}$. The parameters given in the above-mentioned kernels are defined as follows:

$$\begin{aligned} &\alpha(\omega) = \left[1 - \zeta\left(g_{m1}\beta(\omega) - j\omega C_{gs1} g_{m3,p}\right)\lambda(\omega)\right], \\ &\zeta = L_s / C_{gs1}, \\ &\beta(\omega) = Z_1^{-1}(\omega) + j\omega C_{gs3,p}, \\ &\beta(2\omega_b) = Z_1^{-1}(2\omega_b) + 2j\omega_b C_{gs3,p}, \\ &\gamma(\omega) = j\omega C_{gs1} + (j\omega L_s)^{-1} + g_{m1}, \\ &\lambda(\omega) = (1 + \zeta\gamma(\omega)\beta(\omega))^{-1}, \\ &A_1(\omega) = \left(j\omega Z_1 C_{gs1} + j\omega L_s\left(1 + j\omega Z_1 C_{gs3,p}\right)\gamma(\omega)\right)^{-1} \end{aligned} \tag{22}$$

where $g_{m1} = g_{m1,p}$, $C_{gs1} = C_{gs1,p}$ for the proposed LNA, and $g_{m1} = g_{m1,c}$, $C_{gs1} = C_{gs1,c}$ for the conventional LNA. Moreover, the $g_{m3,p}$, $g'_{m3,p}$, $g''_{m3,p}$

and $C_{gs3,p}$ parameters are zero for the conventional LNA. The detailed linearity analysis is provided in Appendix A. To compare the linearity, it is important to note that the IIP3 is inversely proportional to $|A_1(\pm\omega_b)|^2$, and $A_1(\pm\omega_b)$ is inversely proportional to the $C_{gs3,p}$. Accordingly, the C_b capacitor placed across the gate-source of M_3 transistor is employed to improve the linearity in the proposed LNA. Actually, the IIP3 of the proposed LNA is degraded in comparison with the conventional LNA and C_b is utilized to compensate the IIP3 degradation. The effect of the added C_b capacitor on the linearity and gain will be more explained in Section 3 using the simulation results.

3. Post-layout simulation results

To examine the effectiveness of the proposed LNA, the circuit shown in Fig. 1 has been simulated in Cadence Spectre-RF using TSMC 180 nm CMOS process along with the conventional cascode CS LNA with inductive source degeneration. It has been designed for 2.4 GHz input signal frequency with 100 MHz bandwidth and 1.2 V power supply. The value of designed device components is also shown in Fig. 1. Spiral inductors, metal–insulator-metal (MIM) capacitors and poly resistors are utilized as the passive device components. It is worth mentioning that in the conventional LNA, the size of M_1 transistor is twice that of M_1 which is used in the proposed LNA. For a fair comparison, both LNAs have been designed with the same power consumption. So, the effect of adding M_3 transistor can be seen well. The layout of the proposed and conventional LNAs is illustrated in Fig. 4.

Fig. 5(a) shows the simulated power gain (S_{21}) of the proposed and conventional LNAs over the frequency range of 2.2–2.6 GHz. The maximum S_{21} occurs at 2.45 GHz which is equal to 15.55 dB and 13 dB for the proposed and conventional LNAs, respectively. In other words, the absolute value of power gain in the proposed LNA is 6 while it is 4.47 in the conventional structure showing 34.2 % power gain improvement. In order to represent the accuracy of the input matching network, the input reflection coefficient (S_{11}) of the LNAs is simulated and the results are illustrated in Fig. 5(b). Over the frequency bandwidth of 2.4–2.5 GHz, S_{11} of the proposed and conventional LNAs is less than −12.7 dB and −15.15 dB, respectively.

Fig. 6 presents the simulated noise figure of the proposed LNA in comparison with the conventional cascode CS LNA with inductive source degeneration. The proposed LNA achieves a low NF of 2.42 dB at 2.45 GHz which is 0.06 dB smaller than the NF of the conventional LNA. The minimum achieved NF is 2.16 dB and 2.31 dB for the proposed and conventional LNAs, respectively.

In order to simulate the linearity behavior of the proposed and conventional LNAs, a two-tone RF input signal is applied at 2.449 GHz and 2.451 GHz frequencies with 2 MHz frequency offset to extract the value of in-band IIP3. As mentioned in Section 2.3, the capacitor C_b which is in parallel with C_{gs} of the M_3 transistor, is added for the sake of IIP3 improvement. Fig. 7 illustrates the simulated IIP3 as well as S_{21} of the proposed LNA versus the capacitor C_b. According to this figure, without C_b, the IIP3 of the proposed LNA is −0.23 dBm. The value of IIP3 is enhanced by increasing the value of C_b capacitor as theoretically estimated in linearity analysis. However, the value of S_{21} is slightly reduced when the value of C_b capacitor is increased. Therefore, there is a trade-off between the linearity and power gain, and the value of C_b capacitor can be selected accordingly. In this design, the value of C_b capacitor has been selected as 45 fF in order to have the same 0.84 dBm IIP3 in both proposed and conventional LNAs.

Fig. 8(a) and Fig. 8(b) show the output power against the input power for the both fundamental and third-order intermodulation (IM3) components in the conventional and proposed LNAs, respectively. The achieved IIP3 for both proposed and conventional LNAs is 0.84 dBm. Here, a two-tone RF input signal has been also applied at 2.449 GHz and 2.451 GHz frequencies with 2 MHz frequency offset.

Considering process corner cases, voltage, and temperature (PVT) variations, the operation of the proposed and conventional cascode CS LNAs have been simulated in different states of TT at 27 °C and V_{DD}, SS at 85 °C and $0.9V_{DD}$, and FF at −40 °C and $1.1V_{DD}$. The simulation results are summarized in Table 1 confirming a robust performance over PVT variations.

The stability of the proposed LNA is almost the same as the conventional cascode CS LNA. As well-known [22], the most popular technique to improve the stability of a CS amplifier with an inductive load is the cascode configuration. In cascode structure, the reverse isolation is enhanced and the Miller effect of C_{gd} of the input CS transistor, which is the main instability issue, is highly reduced. In the proposed LNA, the added transistor is placed in parallel with the input transistor of the conventional cascode LNA which is forming only a feedforward path. Therefore, the structure of the proposed LNA is also cascode, and hence, it is inherently stable. To examine the stability, the following factors are mainly utilized [22]:

$$K = \frac{1 + |\Delta|^2 - |S_{11}|^2 - |S_{22}|^2}{2|S_{21}||S_{12}|} \qquad \Delta = S_{11}S_{22} - S_{12}S_{21} \tag{23}$$

If $K > 1$ and $\Delta < 1$, then the LNA is unconditionally stable [22]. Stability factors of the simulated LNAs over wide frequency range of 0.001–50 GHz are illustrated in Fig. 9. At 2.45 GHz, K is 16.6 and 24 for the proposed and conventional LNAs, respectively. Also, at 2.45 GHz, Δ is 0.015 and 0.008 for the proposed and conventional LNAs, respectively. Therefore, the stability condition is established for both structures as well in wide frequency range. Indeed, according to Fig. 9, the plots of K and Δ are almost identical for both LNAs, indicating almost the

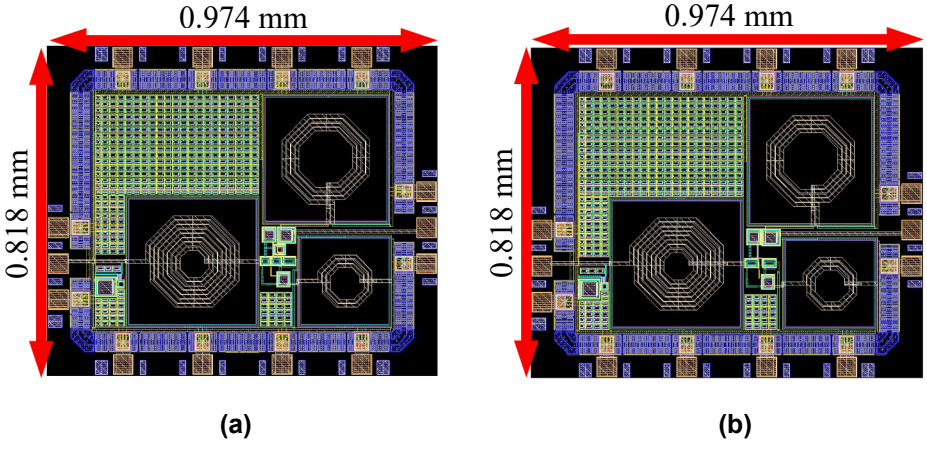

Fig. 4. Layout of the (a) proposed, and (b) conventional LNAs.

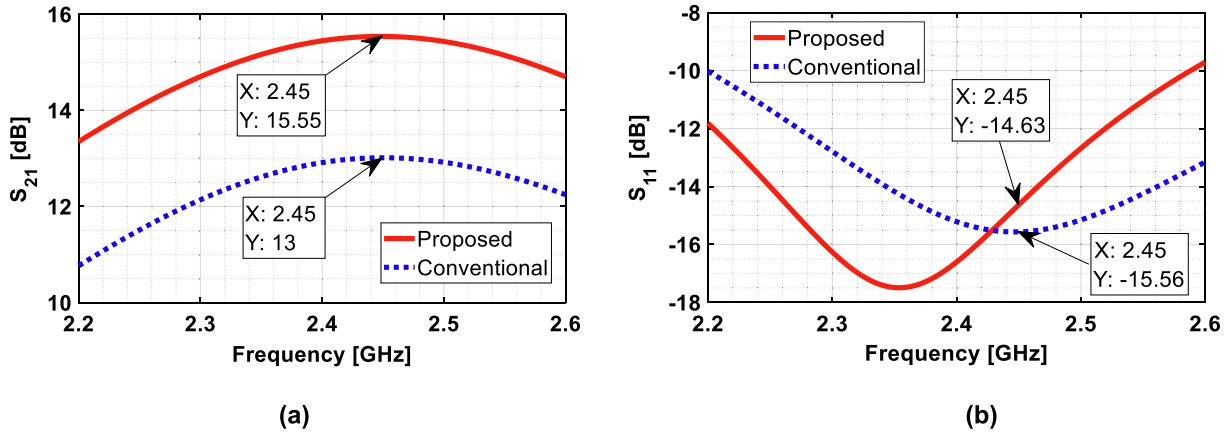

Fig. 5. Simulated (a) S_{21}, and (b) S_{11} of the proposed and conventional LNAs.

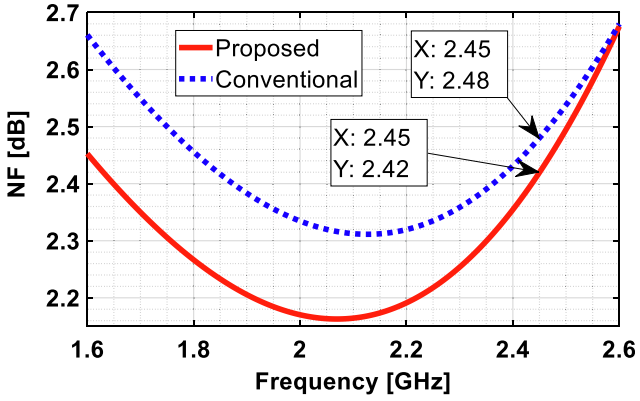

Fig. 6. Simulated NF of the proposed and conventional LNAs.

same stability performance for both LNAs.

In order to examine the effects of process variations and device mismatches on the operation of the proposed LNA, some Monte Carlo simulations have been performed for the S_{21} at 2.45 GHz and IIP3, and the results are illustrated in Fig. 10. The mean value of the power gain in the proposed LNA is 15.52 dB with 0.396 dB standard deviation which means that S_{21} has little changes with the process variations and device mismatches. Also, the mean value of the IIP3 is 0.8 dBm with a standard deviation of 0.261 dBm.

Table 2 summarizes the simulation results of the proposed LNA and compares it with the conventional cascode CS LNA with inductive source degeneration and several published state-of-the-art works. The following figure of merit (FoM) is also used to compare the proposed LNA with several published LNAs [33,34]:

$$FoM[GHz] = \frac{10^{\frac{Power\ \ Gain\ \ [dB]}{20}} \times 10^{\frac{IIP3[dBm]}{10}} \times f_0[GHz]}{\left(10^{\frac{NF[dB]}{10}} - 1\right) \times P_{DC}[mW]} \quad (24)$$

where f_0 is the central frequency of LNA. As it is clear, in equal P_{DC}, IIP3, and area, the absolute amount of the power gain in the proposed LNA is 6 while it is 4.47 in conventional structure showing 34.2 % power gain improvement. The NF of the proposed LNA is slightly lower than the conventional one. The achieved FoM of the proposed LNA is substantially greater than the conventional cascode LNA. In other words, the FoM has been improved by 38.4 % in comparison to the conventional cascode CS LNA with inductive source degeneration.

In [14,15,38], several additional techniques have been used in the CS LNA to improve the overall performance resulting in larger FoM in comparison with other LNAs listed in Table 2. In [14], the linearity of a sub-threshold cascode CS LNA with inductive source degeneration has been improved by reducing the third-order distortion. The tunable negative feedback capacitor, forward body biasing, input feedback capacitor, multiple-gate, and current reuse techniques have been employed in the basic CS LNA with inductive source degeneration in [15] to realize a variable gain LNA. In [38], a push–pull CS LNA structure with inductive source degeneration has been utilized for passive gain boosting with preserved good linearity at low power consumption.

It is worth mentioning that the proposed idea has been employed in the basic structure of the conventional cascode CS LNA with inductive source degeneration. It can be also utilized in all improved CS LNAs with inductive source degeneration like [14,15,38] to further improve the

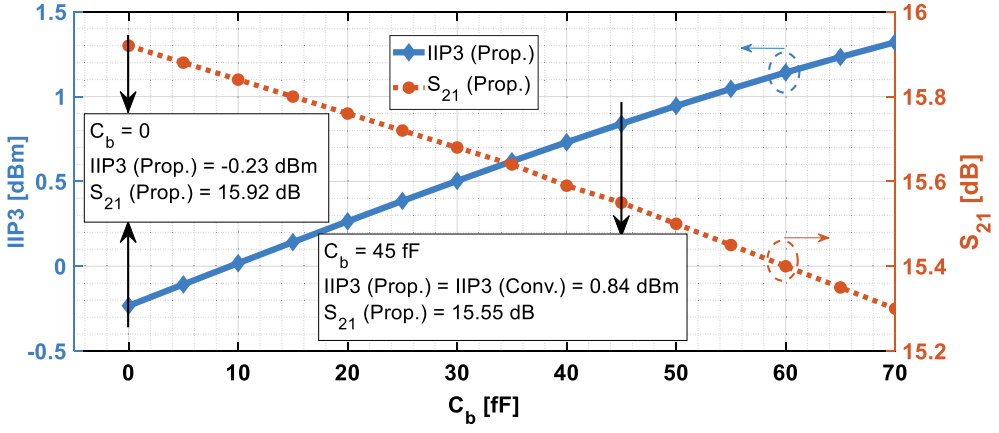

Fig. 7. Simulated IIP3 and S_{21} of the proposed LNA as a function of C_b capacitor.

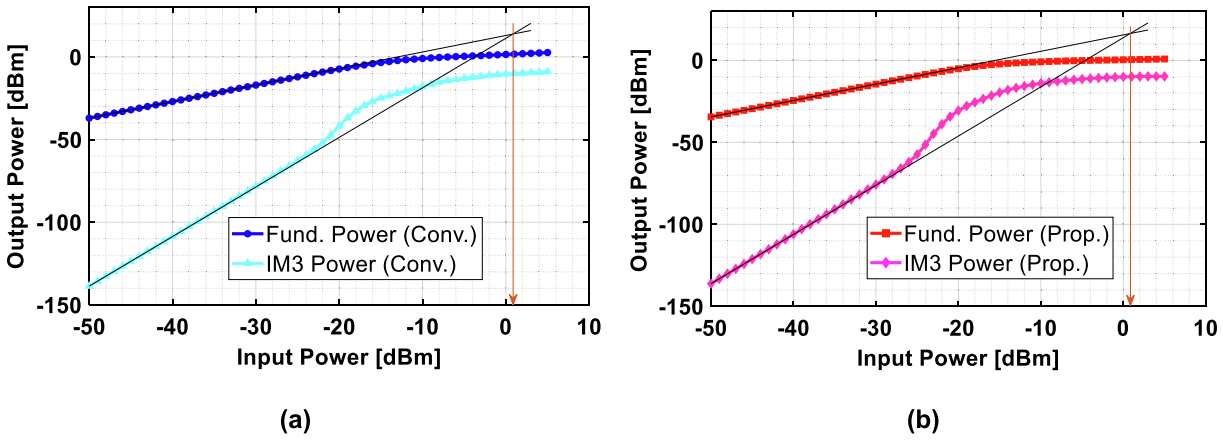

Fig. 8. Simulated IIP3 of (a) conventional, and (b) proposed LNAs.

Table 1
Simulated performance of the LNAs over PVT variations.

Parameter	SS @ 85 °C & 0.9V_{DD}		TT @ 27 °C & V_{DD}		FF @ −40 °C & 1.1V_{DD}	
	Proposed LNA	Conventional LNA	Proposed LNA	Conventional LNA	Proposed LNA	Conventional LNA
P_{DC} [mW]	2.52	2.53	3.2	3.2	3.92	3.92
S_{21} [dB]	13.54	11.4	15.55	13	17.9	14.88
NF [dB]	3.08	3.17	2.42	2.48	1.71	1.74
S_{11} [dB]	<−12.1	<−15.93	<−12.7	<−15.15	<−12.38	<−13.46
IIP3 [dBm]	−0.04	0.22	0.84	0.84	0.51	1.13

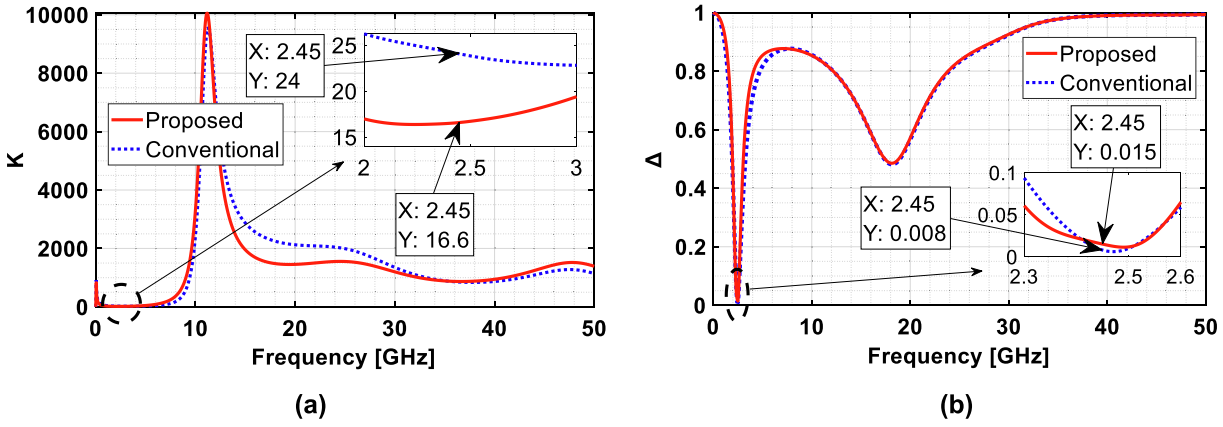

Fig. 9. Simulated (a) Stern stability factor *K*, and (b) Δ for the proposed and conventional LNAs.

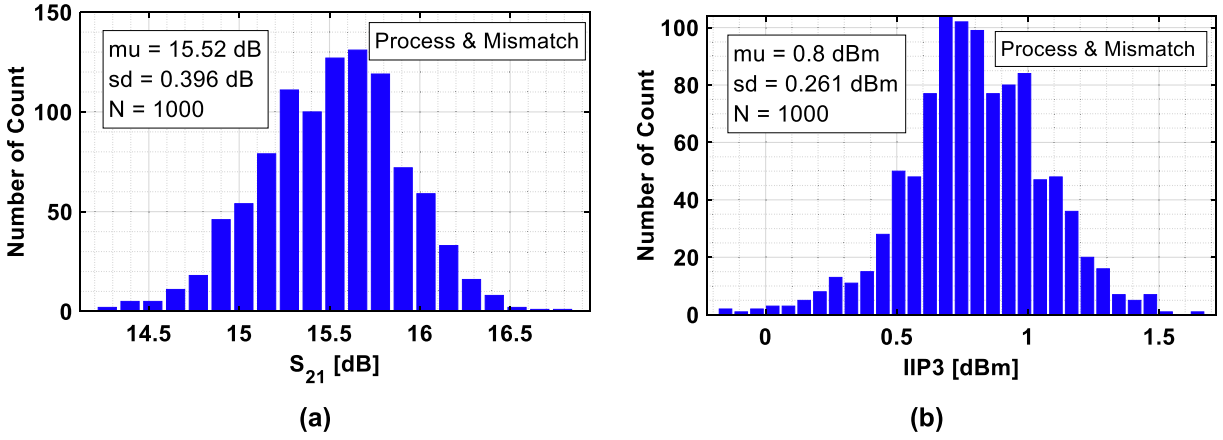

Fig. 10. Monte Carlo simulation results of the proposed LNA for (a) S_{21}, and (b) IIP3.

Table 2
Performance comparison with several narrow-band CMOS LNAs.

Reference	Tech. [nm]	Freq. [GHz]	NF [dB]	S_{21} [dB]	S_{11} [dB]	IIP3 [dBm]	P_{DC} [mW]	Area [mm^2]	FoM [GHz]
Proposed LNA*	180	2.45	2.42	15.55	<−12.7	0.84	3.2	0.796[d]	7.46
Cascode CS LNA*	180	2.45	2.48	13	<−15.15	0.84	3.2	0.796[d]	5.39
ISCAS'20 [13]*	180	1.8	4	13	−55	5.5	10.8	–	1.75
TCAS-I'18 [14]	110	1.8	3.7	14.8	<−10	−3.7	0.336	0.623[e]	9.34
TCAS-II'20 [15]	180	2.8	4	10[a]	−9	0	0.6	0.9[d]	9.76
TCAS-I'19 [16]	180	2.4	3.25	10.8	−15	4.5	11.7	1.034[d]	1.8
IA'17 [17]*	130	2.4	3.2	19.3	−16.8	−20.1	2.4	–	0.08
TMTT'17 [18]	130	3	2.5[b]	21.2[a]	−10.4[c]	−12.5	7.2	–	0.35
IA'19 [19]*	55	2.45	2.6	16.78	−16.37	−12.66	3.75	0.83[e]	0.3
JSSC'18 [23]	65	2.4	2.8	17.4	<−13.5	−10.7	0.475	0.42[e]	3.52
AEUE'20 [24]*	180	2.4	3.1	10.6	−6.9	−2.7	16.5	1.767[e]	0.25
TCAS-II'19 [35]	180	2.4	3.46	10.4	−9.2	−8.4	1.31	1.63[d]	0.72
NewCAS'18 [36]	130	2.4	5.05	13.8	<−10	−13	0.08	–	3.35
ISCAS'20 [37]	180	2.6	3	16.5	–	−16	0.6	1.2[d]	0.73
JSSC'20 [38]	65	2.4	6.8	11	<−20	−2.2	0.174	–	7.79
AEUE'09 [39]**	250	2	4	25.67	−14.6	–	5.13	–	–
AEUE'21 [40]*	180	2.4	3.45	14	<−11	−8	0.98	0.375[e]	1.6

* Post-layout simulation results.
** Schematic-level simulation results.
[a] Maximum power gain.
[b] Minimum NF.
[c] Minimum S_{11}.
[d] Including pads.
[e] Excluding pads.

achieved FoM since it increases the power gain with almost the same other performance parameters.

4. Conclusion

By adding an extra transistor to the conventional cascode CS LNA with inductive source degeneration, a new LNA structure is proposed to improve the power gain substantially almost with the same other performance parameters. Also, an additional capacitor is placed between the gate-source of the added transistor to avoid the IIP3 reduction in comparison with the conventional LNA. Detailed post-layout simulation results confirm that the power gain of the proposed LNA is increased 34.2 % compared to the conventional cascode CS LNA with the same power consumption, IIP3, and area. The proposed technique can be utilized in all recently improved CS LNAs with inductive source degeneration to further enhance the power gain without needing additional power consumption and area and also degradation in IIP3 and other performance metrics.

Declaration of Competing Interest

The authors declare that they have no known competing financial interests or personal relationships that could have appeared to influence the work reported in this paper.

Data availability

No data was used for the research described in the article.

Acknowledgement

This work has been financially supported in part by Iran National Science Foundation (INSF) under the contract number of 99011612.

Appendix A. Linearity analysis by means of the Volterra series method

As it mentioned before, the schematic of Fig. 2 is used for linearity analysis. In this analysis, $C_{gs1} = C_{gs,M1} + C_a$, and $C_{gs3} = C_{gs,M3} + C_b$, where C_a and C_b are the added capacitors in parallel with the gate-source of M_1 and M_3 transistors, and, $C_{gs,M1}$ and $C_{gs,M3}$ are the gate-source capacitances of M_1 and M_3 transistors, respectively.

According to Fig. 2, the output current can be written as:

$$i_{out} = i_a + i_b = g_{m1}v_a + \frac{g'_{m1}}{2}v_a^2 + \frac{g''_{m1}}{6}v_a^3 + g_{m3}v_b + \frac{g'_{m3}}{2}v_b^2 + \frac{g''_{m3}}{6}v_b^3$$
$$I_{out} \triangleq E_1(\omega)^\circ V_{in} + E_2(\omega_1,\omega_2)^\circ V_{in}^2 + E_3(\omega_1,\omega_2,\omega_3)^\circ V_{in}^3 \quad (A.1)$$

where E_1, E_2, and E_3 are 1st, 2nd, and 3rd order Volterra series kernels of the output current. By substituting the relation (17) into (A.1) and neglecting the terms V_{in}^4 and beyond, we have:

$$E_1(\omega) = g_{m1}A_1(\omega) + g_{m3}B_1(\omega) \quad (A.2)$$

$$E_2(\omega_1,\omega_2) = g_{m1}A_2(\omega_1,\omega_2) + \frac{g'_{m1}}{2}A_1(\omega_1)A_1(\omega_2) + g_{m3}B_2(\omega_1,\omega_2) + \frac{g'_{m3}}{2}B_1(\omega_1)B_1(\omega_2) \quad (A.3)$$

$$E_3(\omega_1,\omega_2,\omega_3) = g_{m1}A_3(\omega_1,\omega_2,\omega_3) + g'_{m1}\overline{A_1(\omega_1)A_2(\omega_2,\omega_3)} + \frac{g''_{m1}}{6}A_1(\omega_1)A_1(\omega_2)A_1(\omega_3) + g_{m3}B_3(\omega_1,\omega_2,\omega_3) + g'_{m3}\overline{B_1(\omega_1)B_2(\omega_2,\omega_3)} + \frac{g''_{m3}}{6}B_1(\omega_1)B_1(\omega_2)B_1(\omega_3) \tag{A.4}$$

where the bar indicates the averaging function which is defined as follows:

$$\overline{A_1(\omega_1)A_2(\omega_2,\omega_3)} = \frac{1}{3}[A_1(\omega_1)A_2(\omega_2,\omega_3) + A_1(\omega_2)A_2(\omega_1,\omega_3) + A_1(\omega_3)A_2(\omega_1,\omega_2)] \tag{A.5}$$

Assuming that the fundamental response is placed at ω_a, and defining $v_{in} = A(\cos(\omega_a t) + \cos(\omega_b t))$ for a two-tone excitation, the input tone amplitude at the intercept point of the IM3 response at $\pm 2\omega_b \mp \omega_a$ can be formulated as:

$$A_{IP3}(\pm 2\omega_b \mp \omega_a) = \sqrt{\frac{4}{3}\left|\frac{E_1(\omega_a)}{E_3(\pm\omega_b,\pm\omega_b,\mp\omega_a)}\right|} \tag{A.6}$$

Moreover, the IIP3, the available power at the 3rd order intercept point, can be stated as:

$$IIP3(\pm 2\omega_b \mp \omega_a) = \frac{A^2_{IP3}(\pm 2\omega_b \mp \omega_a)}{8Re(Z_1(\omega_a))} = \frac{1}{6Re(Z_1(\omega_a))}\left|\frac{E_1(\omega_a)}{E_3(\pm\omega_b,\pm\omega_b,\mp\omega_a)}\right| \tag{A.7}$$

where $\omega_1 = \omega_2 = \pm\omega_b$, and $\omega_3 = \mp\omega_a$. The method for achieving A_1, A_2, A_3, as well as B_1, B_2, and B_3 parameters is by solving the Kirchhoff's law equations, in the frequency domain, at the gate and source terminals of transistor M_1 in Fig. 2. These equations are given in the relations (A.8) and (A.9) as:

$$\frac{V_b - V_{in}}{Z_1} + j\omega\, V_b C_{gs3} + j\omega\, V_a C_{gs1} = 0 \tag{A.8}$$

$$-j\omega\, V_a C_{gs1} + \frac{V_b - V_a}{j\omega L_s} - g_{m1}V_a - \frac{g'_{m1}}{2}V_a^2 - \frac{g''_{m1}}{6}V_a^3 = 0 \tag{A.9}$$

Substituting Eq. (17) into Eq. (A.8) and Eq. (A.9), the B_1 and A_1 regarding the first order term of the excitation voltage are calculated as Eq. (A.10) and Eq. (A.11), respectively.

$$B_1(\omega) = j\omega\, L_s\left[g_{m1} + \frac{1}{j\omega\, L_s} + j\omega\, C_{gs1}\right]A_1(\omega) \tag{A.10}$$

$$A_1(\omega) = \left(j\omega\, Z_1 C_{gs1} + j\omega\, L_s(1 + j\omega\, Z_1 C_{gs3})\left[g_{m1} + \frac{1}{j\omega\, L_s} + j\omega\, C_{gs1}\right]\right)^{-1} \tag{A.11}$$

In the same manner, the B_2 and A_2 are calculated as Eq. (A.12) and Eq. (A.13), respectively.

$$B_2(\omega_1,\omega_2) = \frac{\frac{1}{2}[j(\omega_1+\omega_2)L_s][g'_{m1}A_1(\omega_1)A_1(\omega_2)]}{1 + \left[\left\{g_{m1} + \frac{1}{j(\omega_1+\omega_2)L_s} + j(\omega_1+\omega_2)C_{gs1}\right\}\left(\frac{1}{Z_1(\omega_1,\omega_2)} + j(\omega_1+\omega_2)C_{gs3}\right)\right]\frac{L_s}{C_{gs1}}} \tag{A.12}$$

$$A_2(\omega_1,\omega_2) = \frac{-\left(\frac{1}{Z_1(\omega_1,\omega_2)} + j(\omega_1+\omega_2)C_{gs3}\right)}{j(\omega_1+\omega_2)C_{gs1}}B_2(\omega_1,\omega_2) \tag{A.13}$$

Likewise, the expressions for the 3rd order terms, B_3 and A_3, are calculated as:

$$B_3(\omega_1,\omega_2,\omega_3) = \frac{j\omega_{1,2,3}L_s\left[g'_{m1}\overline{A_1(\omega_1)A_2(\omega_2,\omega_3)} + \frac{g''_{m1}}{6}A_1(\omega_1)A_1(\omega_2)A_1(\omega_3)\right]}{1 + \left\{g_{m1} + \frac{1}{j\omega_{1,2,3}L_s} + j\omega_{1,2,3}C_{gs1}\right\}\left\{\frac{1}{Z_1(\omega_1,\omega_2,\omega_3)} + j\omega_{1,2,3}C_{gs3}\right\}\frac{L_s}{C_{gs1}}} \tag{A.14}$$

$$A_3(\omega_1,\omega_2,\omega_3) = \frac{-\left(\frac{1}{Z_1(\omega_1,\omega_2,\omega_3)} + j\omega_{1,2,3}C_{gs3}\right)}{j\omega_{1,2,3}C_{gs1}}B_3(\omega_1,\omega_2,\omega_3) \tag{A.15}$$

where $\omega_{1,2,3}$ means $\omega_1 + \omega_2 + \omega_3$. With the assumption that these frequencies are closely spaced, i.e. $\omega_a \approx \omega_b \approx \omega$, we can write $\omega_1 + \omega_2 + \omega_3 = \omega_{1,2,3} = \pm 2\omega_b \mp \omega_a \approx \pm\omega$. In this manner, from Eq. (A.12), B_2 and A_2 can be rewritten as Eq. (A.16).

$$B_2(\pm\omega_b,\mp\omega_a) = \frac{\frac{1}{2}[j\Delta\omega L_s][g'_{m1}A_1(\pm\omega_b)A_1(\mp\omega_a)]}{1 + \left[\left\{g_{m1} + \frac{1}{j\Delta\omega L_s} + j\Delta\omega C_{gs1}\right\}\left(\frac{1}{Z_1(\pm\omega_b,\mp\omega_a)} + j\Delta\omega C_{gs3}\right)\right]\frac{L_s}{C_{gs1}}}$$
$$B_2(\pm\omega_b,\pm\omega_b) = \frac{\frac{1}{2}[\pm 2j\omega_b L_s][g'_{m1}A_1(\pm\omega_b)A_1(\pm\omega_b)]}{1 + \left[\left\{g_{m1} \pm \frac{1}{2j\omega_b L_s} \pm 2j\omega_b C_{gs1}\right\}\left(\frac{1}{Z_1(\pm\omega_b,\pm\omega_b)} \pm 2j\omega_b C_{gs3}\right)\right]\frac{L_s}{C_{gs1}}} \tag{A.16}$$

As we have assumed that frequencies are closely spaced, we have $\Delta\omega = \pm\omega_b \mp \omega_a \approx 0$. As a result,$B_2(\omega_b,-\omega_a) \approx 0$. In addition, based on Eq.

(A.13), we can say $A_2(\omega_b,-\omega_a)\approx 0$ as well. In continuation of calculating the B_2 parameters, A_2 is calculated as Eq. (A.17) by combining Eq. (A.12) and Eq. (A.13).

$$A_2(\pm\omega_b,\pm\omega_b)=\frac{-\left(\frac{1}{Z_1(\pm\omega_b,\pm\omega_b)}\pm 2j\omega_b C_{gs3}\right)}{\pm 2j\omega_b C_{gs1}}B_2(\pm\omega_b,\pm\omega_b)=\frac{-\frac{1}{2}\left[\frac{L_s}{C_{gs1}}\right]\left[g_{m1}^{'}A_1(\pm\omega_b)A_1(\pm\omega_b)\right]\left(\frac{1}{Z_1(\pm\omega_b,\pm\omega_b)}\pm 2j\omega_b C_{gs3}\right)}{1+\frac{L_s}{C_{gs1}}\left[\left\{g_{m1}\pm\frac{1}{2j\omega_b L_s}\pm 2j\omega_b C_{gs1}\right\}\left(\frac{1}{Z_1(\pm\omega_b,\pm\omega_b)}\pm 2j\omega_b C_{gs3}\right)\right]} \tag{A.17}$$

By combining Eq. (A.5) and Eq. (A.17), we have:

$$\overline{A_1(\pm\omega_b)A_2(\pm\omega_b,\mp\omega_a)}=\frac{1}{3}A_1(\mp\omega_a)A_2(\pm\omega_b,\pm\omega_b)=\frac{-\frac{1}{6}A_1(\mp j\omega_a)\left[\frac{L_s}{C_{gs1}}\right]\left[g_{m1}^{'}A_1(\pm\omega_b)A_1(\pm\omega_b)\right]\left(\frac{1}{Z_1(\pm\omega_b,\pm\omega_b)}\pm 2j\omega_b C_{gs3}\right)}{1+\frac{L_s}{C_{gs1}}\left[\left\{g_{m1}\pm\frac{1}{2j\omega_b L_s}\pm 2j\omega_b C_{gs1}\right\}\left(\frac{1}{Z_1(\pm\omega_b,\pm\omega_b)}\pm 2j\omega_b C_{gs3}\right)\right]} \tag{A.18}$$

At this point, we make some definitions given in Eq. (A.19) – Eq. (A.24).

$$\gamma(\omega)=j\omega C_{gs1}+(j\omega L_s)^{-1}+g_{m1} \tag{A.19}$$

$$\begin{aligned}&\beta(\omega)=Z_1^{-1}(\omega)+j\omega C_{gs3}\\ &\beta(\pm\omega)=\frac{1}{Z_1(\pm\omega_b,\pm\omega_b,\mp\omega_a)}\pm j(\pm\omega_b\pm\omega_b\mp\omega_a)C_{gs3}=Z_1^{-1}(\pm\omega_b,\pm\omega_b,\mp\omega_a)\pm j\omega C_{gs3}\end{aligned} \tag{A.20}$$

$$\zeta=L_s/C_{gs1} \tag{A.21}$$

$$\begin{aligned}&\lambda(\omega)=(1+\zeta\gamma(\omega)\beta(\omega))^{-1}\\ &\lambda(\pm 2\omega_b)=(1+\zeta\gamma(\pm 2\omega_b)\beta(\pm 2\omega_b))^{-1}\end{aligned} \tag{A.22}$$

$$\gamma(2\omega_b)\triangleq\gamma(2\omega)=2j\omega_b C_{gs1}+(2j\omega_b L_s)^{-1}+g_{m1} \tag{A.23}$$

$$\beta(2\omega_b)\triangleq\beta(2\omega)=Z_1^{-1}(2\omega_b)+2j\omega_b C_{gs3} \tag{A.24}$$

From Eq. (A.14), and Eq. (A.18) – Eq. (A.21), B_3 is calculated as Eq. (A.25).

$$B_3(\pm\omega_b,\pm\omega_b,\mp\omega_a)=\frac{\pm j\omega L_s\left[\frac{-\frac{\zeta}{6}g_{m1}^{'2}A_1(\mp\omega_a)A_1^2(\pm\omega_b)\beta(\pm 2\omega_b)}{1+\zeta\gamma(\pm 2\omega_b)\beta(\pm 2\omega_b)}+\frac{g_{m1}^{''}}{6}A_1^2(\pm\omega_b)A_1(\mp\omega_a)\right]}{1+\zeta\beta(\pm\omega)\gamma(\pm\omega)} \tag{A.25}$$

In addition, using Eq. (A.15), A_3 is calculated from Eq. (A.26) as:

$$A_3(\pm\omega_b,\pm\omega_b,\mp\omega_a)=\frac{-\zeta\Big/6\beta(\pm\omega)\left[\frac{-\zeta g_{m1}^{'2}A_1(\mp\omega_a)A_1^2(\pm\omega_b)\beta(\pm 2\omega_b)}{1+\zeta\gamma(\pm 2\omega_b)\beta(\pm 2\omega_b)}+g_{m1}^{''}A_1^2(\pm\omega_b)A_1(\mp\omega_a)\right]}{1+\zeta\beta(\pm\omega)\gamma(\pm\omega)} \tag{A.26}$$

Considering Eq. (A.10) and Eq. (A.16), we have:

$$\overline{B_1(\pm\omega_b)B_2(\pm\omega_b,\mp\omega_a)}=\frac{\frac{1}{3}\gamma(\mp\omega_a)g_{m1}^{'}\omega_a\omega_b L_s^2}{1+\zeta\beta(\pm 2\omega_b)\gamma(\pm 2\omega_b)}A_1(\mp\omega_a)A_1^2(\pm\omega_b) \tag{A.27}$$

In addition, based on Eq. (A.10), the term $B_1^2(\pm\omega_b)B_1(\mp\omega_a)$ can be simplified as Eq. (A.28).

$$B_1(\omega)=j\omega L_s\gamma(\omega)A_1(\omega)\Rightarrow B_1^2(\pm\omega_b)B_1(\mp\omega_a)=j\omega_a\omega_b^2L_s^3\gamma^2(\pm\omega_b)\gamma(\mp\omega_a)A_1^2(\pm\omega_b)A_1(\mp\omega_a) \tag{A.28}$$

By combining the equations (A.18), (A.25), and (A.26-A.28), and with the assumption of $\omega_a\approx\omega_b\approx\omega$, the 1st and 3rd order Volterra series kernels of the output current, E_1 and E_3 are calculated as Eq. (A.29).

$$E_3(\pm\omega_b,\pm\omega_b,\mp\omega_a)=\frac{1}{6}A_1(\mp\omega_a)A_1^2(\pm\omega_b)\left\{\begin{array}{c}\zeta\left[-\zeta g_{m1}^{'2}\beta(\pm 2\omega_b)\lambda(\pm 2\omega_b)+g_{m1}^{''}\right]\left(\pm j\omega g_{m3}C_{gs1}-g_{m1}\beta(\pm\omega)\right)\lambda(\pm\omega)\\ -\zeta g_{m1}^{'}\lambda(\pm 2\omega_b)\left[g_{m1}^{'}\beta(\pm 2\omega_b)-2g_{m3}^{'}\omega_a\omega_b C_{gs1}L_s\gamma(\mp\omega_a)\right]\\ +g_{m1}^{''}+j\omega_a{\omega_b}^2g_{m3}^{''}L_s^3\gamma^2(\pm\omega_b)\gamma(\mp\omega_a)\end{array}\right\} \tag{A.29}$$

This expression can be further simplified by assuming $\omega_a\approx\omega_b\approx\omega$ as:

$$E_3(\pm\omega_b,\pm\omega_b,\mp\omega_a)=\frac{1}{6}A_1(\mp\omega_a)A_1^2(\pm\omega_b)\left\{\begin{array}{c}\left[g_{m1}^{''}-\zeta g_{m1}^{'2}\beta(\pm 2\omega_b)\lambda(\pm 2\omega_b)\right]\left[1-\zeta\left(g_{m1}\beta(\pm\omega)\mp j\omega C_{gs1}g_{m3}\right)\lambda(\pm\omega)\right]\\ +\left[\omega^2L_s^2\gamma(\mp\omega_a)\right]\left[2g_{m1}^{'}g_{m3}^{'}\lambda(\pm 2\omega_b)+j\omega_b L_s g_{m3}^{''}\gamma^2(\pm\omega_b)\right]\end{array}\right\} \tag{A.30}$$

For calculating E_1, we can use Eq. (A.2) in combination with Eq. (A.10), which is given in Eq. (A.31).

$$E_1(\omega_a)=g_{m1}A_1(\omega_a)+g_{m3}B_1(\omega_a)=A_1(\omega_a)(g_{m1}+j\omega_a L_s\gamma(\omega_a)g_{m3}) \tag{A.31}$$

Finally, using equations (A.7), (A.30), and (A.31), the value of IIP3 is calculated as Eq. (A.32).

$$IIP3(\pm 2\omega_b \mp \omega_a) = \frac{1}{6Re(Z_1(\omega_a))}\left|\frac{E_1(\omega_a)}{E_3(\pm\omega_b,\pm\omega_b,\mp\omega_a)}\right| = \frac{1}{6Re(Z_1(\omega_a))}\left|\frac{A_1(\omega_a)}{A_1(\mp\omega_a)A_1^2(\pm\omega_b)}\right| \times \left|\frac{(g_{m1}+j\omega_a L_s\gamma(\omega_a)g_{m3})}{\left\{\begin{array}{c}[g''_{m1}-\zeta g'^2_{m1}\beta(\pm 2\omega_b)\lambda(\pm 2\omega_b)][1-\zeta(g_{m1}\beta(\pm\omega)\mp j\omega C_{gs1}g_{m3})\lambda(\pm\omega)] \\ +[\omega_a\omega_b L_s^2\gamma(\mp\omega_a)][2g'_{m1}g'_{m3}\lambda(\pm 2\omega_b)+j\omega_b L_s g''_{m3}\gamma^2(\pm\omega_b)]\end{array}\right\}}\right| \quad (A.32)$$

It is worth mentioning that Eq. (A.32) can be used to achieve corresponding IIP3 equations for the proposed and conventional LNAs. Indeed, the following substitutions should be applied to Eqs. (A.19)–(A.24), as well as Eq. (A.32): $g_{m1} = g_{m1,p}$, $g_{m3} = g_{m3,p}$, $C_{gs1} = C_{gs1,p}$, $C_{gs3} = C_{gs3,p}$ for the proposed LNA, and $g_{m1} = g_{m1,c}$, $C_{gs1} = C_{gs1,c}$ for the conventional LNA. Moreover, the g_{m3}, g'_{m3}, g''_{m3} and C_{gs3} parameters are zero for the conventional LNA.

Accordingly, the IIP3 for the proposed and conventional LNAs are finalized as Eq. (A.33) and Eq. (A.34), respectively.

$$IIP3(\pm 2\omega_b \mp \omega_a) = \frac{1}{6Re(Z_1(\omega_a))}\left|\frac{E_1(\omega_a)}{E_3(\pm\omega_b,\pm\omega_b,\mp\omega_a)}\right| = \frac{1}{Re(Z_1(\omega_a))}\left|\frac{A_1(\omega_a)}{A_1(\mp\omega_a)A_1^2(\pm\omega_b)}\right| \times \left|\frac{(g_{m1,p}+j\omega_a L_s\gamma(\omega_a)g_{m3,p})}{\left\{\begin{array}{c}[g''_{m1,p}-\zeta g'^2_{m1,p}\beta(\pm 2\omega_b)\lambda(\pm 2\omega_b)][1-\zeta(g_{m1,p}\beta(\pm\omega)\mp j\omega C_{gs1,p}g_{m3,p})\lambda(\pm\omega)] \\ +[\omega^2 L_s^2\gamma(\mp\omega_a)][2g'_{m1,p}g'_{m3,p}\lambda(\pm 2\omega_b)+j\omega_b L_s g''_{m3,p}\gamma^2(\pm\omega_b)]\end{array}\right\}}\right| \quad (A.33)$$

$$IIP3(\pm 2\omega_b \mp \omega_a) = \frac{1}{6\mathrm{Re}(Z_1(\omega_a))}\left|\frac{E_1(\omega_a)}{E_3(\pm\omega_b,\pm\omega_b,\mp\omega_a)}\right| = \frac{1}{\mathrm{Re}(Z_1(\omega_a))}\left|\frac{A_1(\omega_a)}{A_1(\mp\omega_a)A_1^2(\pm\omega_b)}\right| \times \left|\frac{g_{m1,c}}{\{[g''_{m1,c}-\zeta g'^2_{m1,c}\beta(\pm 2\omega_b)\lambda(\pm 2\omega_b)][1-\zeta g_{m1,c}\beta(\pm\omega)\lambda(\pm\omega)]\}}\right| \quad (A.34)$$

References

[1] Kargaran E, Guo B, Manstretta D, Castello R. A Sub-1-V, 350-μW, 6.5-dB Integrated NF Low-IF Receiver Front-End for IoT in 28-nm CMOS. IEEE Solid-State Circ Lett 2019;2(4):29–32.

[2] Yaghoobi M, Haghi Kashani M, Yavari M, Mirabbasi S. A 56-to-66 GHz CMOS Low-Power Phased-Array Receiver Front-End with Hybrid Phase Shifting Scheme. IEEE Trans Circ Syst-I: Reg Pap 2020;67(11):4002–14.

[3] Guo B, Gong J, Wang Y. A wideband differential linear low-noise transconductance amplifier with active-combiner feedback in complementary MGTR configurations. IEEE Trans Circ Syst I: Reg Pap 2021;68(1):224–37.

[4] Shirmohammadi B, Yavari M. A Linear Wideband CMOS Balun-LNA with Balanced Loads. IEEE Trans Circ Syst-II: Exp Briefs 2022;69(3):754–8.

[5] Sabzi M, Kamarei M, Razban T, Mahe Y. Optimization of LNA's first stage to reduce overall noise figure in multi-stage LNAs. AEU-Int J Electron Commun 2020;123:153300.

[6] Kishore KH, Prakash S, Venkataramani B. 1.2 V asymmetric-CCC based sub-3 dB NF high IIP3 linearity wideband balun-LNA. AEU-Int J Electron Commun 2020;117:153090.

[7] Gladson SC, Bhaskar M. A low power high-performance area efficient RF front-end exploiting body effect for 2.4 GHz IEEE 802.15. 4 applications. AEU-Int J Electron Commun 2018;96:81–92.

[8] Beigi A, Safarian A. Low power receiver with merged N-path LNA and mixer for MICS applications. AEU-Int J Electron Commun 2020;117:153111.

[9] Mazhabjafari B, Yavari M. A UWB CMOS Low-Noise Amplifier with Noise Reduction and Linearity Improvement Techniques. Microelectron J Feb. 2015;46(2):198–206.

[10] Guo B, Wen G, An S. 6.8 mW 15 dBm CMOS common-gate LNA employing post-linearization technique. Electron Lett 2014;50(3):149–51.

[11] Guo B, Prevedelli D, Castello R, Manstretta D. A 0.08 mm 2 1–6.2 GHz receiver front-end with inverter-based shunt-feedback balun-LNA. In: IEEE radio frequency integrated circuits symposium (RFIC); 2020. p. 379–82.

[12] Wu J, Guo B, Wang H, Liu H, Li L, Zhou W. A 2.4 GHz 87 μW low-noise amplifier in 65 nm CMOS for IoT applications. Modern Phys Lett B 2021;35(32):2150485.

[13] Pathak D, Vardhan S, Kumar A, Dutta A. Reconfigurable Concurrent Dual-Band Low Noise Amplifier with Dynamic Output Load Network for Software Defined Radio. In: IEEE int symp circuits and systems (ISCAS); 2020. p. 1–5.

[14] Chang C-H, Onabajo M. Analysis and demonstration of an IIP3 improvement technique for low-power RF low-noise amplifiers. IEEE Trans Circ Syst I: Reg Pap 2018;65(3):859–69.

[15] Hsieh J-Y, Lin K-Y. A 0.6-V Low-Power Variable-Gain LNA in 0.18-μm CMOS Technology. IEEE Trans Circ Syst II: Exp Briefs 2020;67(1):23–6.

[16] Chang WL, Meng C, Ni J-H, Chang K-C, Chang C-K, Lee P-Y, et al. Analytical noise optimization of single-/dual-band MOS LNAs with substrate and metal loss effects of inductors. IEEE Trans Circ Syst I: Reg Pap 2019;66(7):2454–67.

[17] Sattar S, Zulkifli TZA. A 2.4/5.2-GHz concurrent dual-band CMOS low noise amplifier. IEEE Access 2017;5:21148–56.

[18] Singh R, Slovin G, Xu M, Schlesinger T, Bain JA, Paramesh J. A reconfigurable dual-frequency narrowband CMOS LNA using phase-change RF switches. IEEE Trans Microwave Theory Tech 2017;65(11):4689–702.

[19] Wang Y-C, Huang Z-Y, Jin T. A 2.35/2.4/2.45/2.55 GHz Low-Noise Amplifier Design Using Body Self-Biasing Technique for ISM and LTE Band Application. IEEE Access 2019;7:183761–9.

[20] Fan X, Zhang H, Sánchez-Sinencio E. A noise reduction and linearity improvement technique for a differential cascode LNA. IEEE J Solid-State Circ 2008;43(3):588–99.

[21] Shaeffer DK, Lee TH. A 1.5-V, 1.5-GHz CMOS low noise amplifier. IEEE J Solid-State Circ 1997;32(5):745–59.

[22] Razavi B. RF Microelectronics. 2nd ed. Prentice Hall; 2012. p. 284–95.

[23] Rahman M, Harjani R. A 2.4-GHz, Sub-1-V, 2.8-dB NF, 475 μW Dual-Path Noise and Nonlinearity Cancelling LNA for Ultra-Low-Power Radios. IEEE J Solid-State Circ 2018;53(5):1423–30.

[24] Bisht R, Akhtar M, Qureshi S. Design of reconfigurable multi-band low-noise amplifiers for 802.11 ah/b/g and DCS-1800 applications. Int J Electron Commun 2020;120:153201.

[25] Yaghoobi M, Yavari M, Haghi Kashani M, Ghafoorifard H, Mirabbasi S. A 55-to-64 GHz Low-Power Small-Area LNA in 65-nm CMOS with 3.8 dB Average NF and ~12.8 dB Power Gain. IEEE Microwave Wireless Comp Lett 2019;29(2):128–30.

[26] Yaghoobi M, Yavari M, Ghafoorifard H. A 17-to-24 GHz Low-Power Variable-Gain Low-Noise Amplifier in 65-nm CMOS for Phased-Array Receivers. Circ Syst Signal Process 2019;38(12):5448–66.

[27] Aparin V, Larson LE. Modified derivative superposition method for linearizing FET low-noise amplifiers. IEEE Trans Microwave Theory Tech 2005;53(2):571–81.

[28] Kim N, Aparin V, Larson LE. Analysis of IM_3 Asymmetry in MOSFET Small-Signal Amplifiers. IEEE Trans Circ Syst I: Reg Pap 2011;58(4):668–76.

[29] Asghari M, Yavari M. Second-order intermodulation cancelation and conversion-gain enhancement techniques for CMOS active mixers. Int J Circ Theory Appl 2015;43(10):1508–22.

[30] Asghari M, Yavari M. Using the Gate-Bulk Interaction and a Fundamental Current Injection to Attenuate IM3 and IM2 Currents in RF Transconductors. IEEE Trans Very Large Scale Integ (VLSI) Syst 2016;24(1):223–32.

[31] Asghari M, Yavari M. An IIP3 Enhancement Technique for CMOS Active Mixers with a Source-Degenerated Transconductance Stage. Microelectron J 2016;50(4):44–9.

[32] Haghi Kashani M, Asghari M, Yavari M, Mirabbasi S. A +7.6 dBm IIP3 2.4-GHz Double-Balanced Mixer with 10.5 dB NF in 65-nm CMOS. IEEE Trans Circ Syst-II: Exp Briefs 2021;68(10):3214–8.
[33] Brederlow R, Weber W, Sauerer J, Donnay S, Wambacq P, Vertregt M. A mixed-signal design roadmap. IEEE Des Test Comput 2001;18(6):34–46.
[34] Linten D, Thijs S, Natarajan MI, Wambacq P, Jeamsaksiri W, Ramos J, et al. A 5-GHz fully integrated ESD-protected low-noise amplifier in 90-nm RF CMOS. IEEE J Solid-State Circ 2005;40(7):1434–42.
[35] Chang C-H. A forward-body-bias CMOS LNA with ultra-low device junction leakage using intrinsic self-balanced pseudo resistor. IEEE Trans Circ Syst II: Express Briefs 2019;66(4):697–701.
[36] Guitton G, Taris T, De Souza M, Mariano AA. Design of CMOS LNA with the Inversion Coefficient. In: IEEE int new circuits and systems conf (NEWCAS); 2018. p. 182–6.
[37] Hsieh J-Y, Kuo H-C. A 0.45-V Low-Power Image-Rejection Low-Noise Amplifier in 0.18-μm CMOS Technology. In: IEEE int symp circuits and systems (ISCAS); 2020. p. 1–4.
[38] Xu K, Yin J, Mak P-I, Staszewski RB, Martins RP. A Single-Pin Antenna Interface RF Front End Using a Single-MOS DCO-PA and a Push-Pull LNA. IEEE J Solid-State Circ 2020;55(8):2055–68.
[39] Salama MK, Soliman AM. Low-voltage low-power CMOS RF low noise amplifier. AEU-Int J Electron Commun 2009;63(6):478–82.
[40] Rastegari F, Dousti M, Ghalamkari B. A 0.75 V Sub-mW CMOS LNA employing transmitted signal suppression technique in a full-duplex wireless brain-machine interface transceiver. AEU-Int J Electron Commun 2021;132:153632.